Supplementary Information

Low-cost flexible textile electrocatalyst for overall water splitting

Zhen Liu,[a]* Jiamin Lan,[a] Xinnian Xia,[a] Tong Ren,[a] Xuxu Wang,[b] Rui Guo,[b,d]* Weijian Xu,[a] and Shuaijun Pan[a,d]*

[a] College of Chemistry and Chemical Engineering, Hunan University, Changsha 410082, China. E-mail: pansj@hnu.edu.cn, zhenliu68@hnu.edu.cn.

[b] College of Chemistry and Materials Science, Hunan Agricultural University, Changsha 410128, China. E-mail: rguo@hnu.edu.cn.

[c] College of Environmental Science and Engineering Hunan University Changsha 410082, China.

[d] Department of Chemical Engineering, The University of Melbourne, Parkville 3010, Australia

1 Materials and Methods

1.1 Materials

Platinum(II) nitrate hexahydrate ($Pt(NO_3)_2$, 98.0%), commercial Pt/C (20 wt%), potassium hydroxide (KOH, 95.0%), and ruthenium(IV) oxide (RuO_2, 99.9%) were received from Aladdin Chemical Reagent Co. Ltd. Ethanol (99.5%), and isopropanol (99.5%) were purchased from Alfa Aesar. Nafion (5 wt%) was purchased from Dow Chemical Company. All of the reagents were used without further purification. Deionized (DI) water was obtained using a water purification equipment (Dow Chemical Company).

1.2 Pretreatment of cotton fibres (CFs) textile

The CFs could be pulled out from freshly cotton ball. The fresh CFs were dried at room temperature (~20 °C) for ~12 h and at 50 °C for 24 h in a vacuum oven. We hand weave the dried CFs into a square shape (5 × 5 cm) using a piece of glass plate as a hard-template and then cut it into 1 × 1cm size squares.

1.3 Synthesis of Pt_{NP}-pCF and Pt_{SA}-pCF

First, freshly picked cotton was dried (80 °C for 24 h) and then woven into centimeter mesh devices; again, the mesh devices were put into $Pt(NO_3)_2$ solutions with different concentrations and reacted with precursor molecules for 24 h. Pt-CF was generated; finally, Pt-CF was pyrolyzed at 900 °C for 2 h to obtain Pt_{SA}-pCF (lower Pt precursor salts (0.5 mmol L^{-1})) and Pt_{NP}-pCF (higher concentrations (5.0 mmol L^{-1})).

1.4 Synthesis of pCF

Pyrolyzed cotton fibres (pCF) were obtained by the pyrolysis of CFs at 900 °C for 2 h with a heating rate of 5 °C min^{-1} in N_2 atmosphere.

2 Characterization

2.1 Instruments

Scanning electron microscopy (SEM) image was obtained using a Hitachi S-4800 instrument. Transmission electron microscopy (TEM) and high-resolution TEM analyses were performed on a JEOL JEM-2100 instrument. The crystal structure was studied by X-ray diffraction (Rigaku Miniflex II) using Cu Kα radiation (λ = 0.154 nm) and at 45 kV and 40 mA. Fourier transform infrared spectroscopy (FTIR) measurements were performed on an IRAffinity-1 instrument (PerkinElmer). Thermogravimetric (TG) analysis was carried out in N_2 atmosphere on a TGA209F1 thermal analyser with heating rate of 5 °C min^{-1}. The elemental content in the catalyst was analysed by inductively coupled plasma–optical emission spectrometry (ICP-OES)-on an ICP-OES730 instrument. Nitrogen adsorption/desorption analysis was performed on a Porosity Analyzer (ASAP2460) to determine the Brunauer–Emmett–Teller surface area and porosity of the samples. X-ray photoelectron spectroscopy (XPS) and high-resolution XPS measurements were conducted on an Escalab 250 spectrometer for elemental identification. Raman spectroscopy were performed using a micro-Raman spectrometer (inVia StreamLine microscope, Renishaw) with a 532 nm laser source at a power of 1 mW.

2.2 Electrochemical measurement

2.2.1 Preparation of working electrodes

a) Pt_{NP}-pCF, Pt_{NP}-pCF, and pCF working electrodes. The Pt_{SA}-pCF and Pt_{NP}-pCF electrode was fixed by a PEEK electrode holder with a cut 1 cm × 1 cm Pt_{NP}-pCF textile. The preparation process of pCF electrode and Pt_{NP}-pCF electrode is the same.

b) Pt/C, RuO_2, Pt_{SA}-pCF and Pt_{NP}-pCF working electrodes. 4 mg Pt/C, RuO_2, Pt_{SA}-pCF, and Pt_{NP}-pCF powder were dispersed in an EtOH–water (500 + 480 μL) solution under sonication, respectively. Next the Nafion solution (20 μL) was added to obtain a uniform catalyst ink, and then the catalyst ink (5 μL) was dropped cast on the polished and clean glass carbon electrode (d = 3 mm) surface to obtain the Pt/C, RuO_2, Pt_{SA}-pCF and Pt_{NP}-pCF working electrodes, respectively.

2.2.2 Measurement

The measured potentials were all converted against the reversible hydrogen electrode (RHE) by $E_{RHE} = E_{Hg/HgO} + 0.0591\ pH + 0.924$. The catalytic activities were evaluated at room temperature on a CHI660E electrochemical workstation with graphite rod as the counter electrode, saturated Hg/HgO solution as the reference electrode, and working electrode. A scan rate of 5 mV s^{-1} was used for the cyclic voltammetry (CV) and linear scan voltammetry (LSV) studies, and all the LSV were operate with 95% iR-corrected. In addition, 30 cycles were performed to ensure stability of tests. Electrochemical impedance spectroscopy (EIS) measurements were performed at onset potentials of 5 mV and a frequency range of 0.1 Hz -100 kHz.

The electrocatalytic overall water splitting and H_2/O_2 generation were driven in a H-shaped electrolyte cell with two Pt_{NP}-pCF electrodes.

2.3 Formulas of electrochemical reaction

2.3.1 Calculation of the turnover frequency (TOF)

$$\text{TOF per site} = \frac{\text{total hydrogen} \frac{\text{turnover}}{\text{cm}^2} \text{ geometric area}}{\text{active} \frac{\text{sites}}{\text{cm}^2} \text{ geometric area}}$$

TOF for HER. The total number of hydrogen turnover was calculated using the following equation:

$$\text{j} \frac{\text{mA}}{\text{cm}^2} \times \frac{\frac{1\text{C}}{\text{s}}}{1000 \text{ mA}} \times \frac{1 \text{ mol e}^-}{96485 \text{ C}} \times \frac{1 \text{ mol H}_2}{2 \text{ mol e}^-} \times \frac{6.02 \times 10^{23} \text{mol H}_2}{1 \text{ mol H}_2} \times 3.12 \times 10^{15} \frac{\frac{\text{H}_2}{\text{s}}}{\text{cm}^2} \text{ per } \frac{\text{mA}}{\text{cm}^2}$$

$$= \text{j} \times 3.12 \times 10^{15} \frac{\text{H}_2/\text{s}}{\text{cm}^2}$$

The total amount of platinum in Pt_{NP}-pCF was determined to be 8.65 wt (Table S1).

Therefore, the density of active sites for HER based on the Pt content was calculated as:

$$\frac{8.65}{159.1} \times \frac{1 \text{ mmol}}{100 \text{ mg}} \times 0.02 \frac{\text{mg}}{\text{cm}^2} \times 6.022 \times 10^{20} \frac{\text{sites}}{\text{mmol}} = 6.548 \times 10^{15} \text{ sites cm}^{-2}$$

For example, the TOF of the catalyst for HER at an overpotential of 200 mV (j = 104.94 mA cm^{-2}) can be calculated as:

$$\text{TOF} = \frac{104.94 \times 3.12 \times 10^{15} \frac{\text{H}_2/\text{s}}{\text{cm}^2}}{6.548 \times 10^{15} \text{ sites cm}^{-2}} = 50.00 \text{ s}^{-1}$$

TOF for OER. The total number of oxygen turnover was calculated using the following equation:

$$\text{j} \frac{\text{mA}}{\text{cm}^2} \times \frac{\frac{1\text{C}}{\text{s}}}{1000 \text{ mA}} \times \frac{1 \text{ mol e}^-}{96485 \text{ C}} \times \frac{1 \text{ mol O}_2}{4 \text{ mol e}^-} \times \frac{6.02 \times 10^{23} \text{mol O}_2}{1 \text{mol O}_2} \times 1.56 \times 10^{15} \frac{\frac{\text{O}_2}{\text{s}}}{\text{cm}^2} \text{ per } \frac{\text{mA}}{\text{cm}^2}$$

$$= \text{j} \times 1.56 \times 10^{15} \frac{\text{O}_2/\text{s}}{\text{cm}^2}$$

Therefore, the density of active sites for OER based on the Pt content was calculated as:

$$\frac{8.65}{159.1} \times \frac{1 \text{ mmol}}{100 \text{ mg}} \times 0.02 \frac{\text{mg}}{\text{cm}^2} \times 6.022 \times 10^{20} \frac{\text{sites}}{\text{mol}} = 1.505 \times 5 \text{ sites cm}^{-2}$$

For example, the TOF of the catalyst for OER at an overpotential of 300 mV (j = 13.77 mA cm^{-2}) was calculated as:

$$\text{TOF} = \frac{13.77 \times 1.56 \times 10^{15} \frac{\text{O}_2/\text{s}}{\text{cm}^2}}{1.505 \times 10^{16} \text{ sites cm}^{-2}} = 14.27 \text{ s}^{-1}$$

2.3.2 Electrochemically active surface area (ECSA)

The ECSA of the prepared catalyst was investigated by calculating the double-layer capacitance (C_{dl}) by recording the CV curve with the non-Faradic region at different scan rates (20–120 mV s^{-1}). The slope of the capacitive current ($\Delta j = j_{anode} - j_{cathode}$) at a given scan rate was double the C_{dl}, which was directly proportional to the ECSA:

$$\mathrm{ECSA} = \frac{C_{dl}}{C_s}$$

where C_s is the specific capacitance (0.040 mF cm^{-2})[1]. The LSV curves were normalized by the ECSA according to the following equation:

$$j_{ECSA} = \frac{j}{\mathrm{ECSA}}$$

3 Theoretical analysis

The plane-wave Density Functional Theory (DFT) calculations were conducted using the Cambridge Sequential Total Energy Package (CASTEP) (an Ab Initio Total Energy Program, Code version: 6546) with the hydrogen binding energy calculated from different active phases[2]. The generalized gradient approximation (GGA) method and revised Perdew-Burke-Ernzerhof (RPBE) functional were applied to treat the electron exchange correlation interaction. The band energy tolerance and DOS k-point separation were 1.0 $\times 10^{-5}$ and 0.03 $Å^{-1}$, respectively. A 3×3×1 Monkhorst–Pack grid k-points and a plane wave basis set cut-off energy of 400 eV were used for integration of the Brillouin zone. The structures were optimized for force and energy convergence set at 2.0×10^{-5} eV and 0.03 $eVÅ^{-1}$, respectively, and a self-consistence field (SCF) of 2.0×10^{-6} eV/atom. A large vacuum space of 15 Å was applied along the direction normal to the catalyst

surface to avoid periodic interactions. To consider the influence of van der Waals interaction, the semi-empirical DFT-D force-field approach was applied.

The Gibb's free energy for hydrogen absorption $|\Delta G_{H^*}|$ were calculated as:

$\Delta G_{H^*} = \Delta E_{H^*} + \Delta ZPE - T\Delta S$

$\Delta E_{H^*} = (E_{(PtNP\text{-}pCF+H^*)} - E_{(PtNP\text{-}pCF} - \frac{1}{2}E_{H_2})$

Where the symbols represent the binding energy (ΔE), the change in zero-point energy (ΔE_{ZPE}), Temperature (T), and the entropy change (ΔS), respectively.

The approximation that the vibrational entropy of hydrogen in the adsorbed state is negligible was applied, whereby $\Delta S_H \approx S_{H^*} - 1/2(S_{H_2}) \approx -1/2(S_{H_2})$, S_{H_2} is the entropy of $H_{2(g)}$ at standard conditions and $TS_{(H_2)}$ is ~0.41 eV for H_2 at 300 K and 1 atm[3].

4 Statistical Analysis

We performed statistical analysis of the size distribution of Pt NPs loaded on cotton fibers using Image J software. For sample, >50 NPs were analyzed and a Gaussian normal distribution analysis was performed using Origin to generate the particle size distribution graphs.

5 Supplemental figures

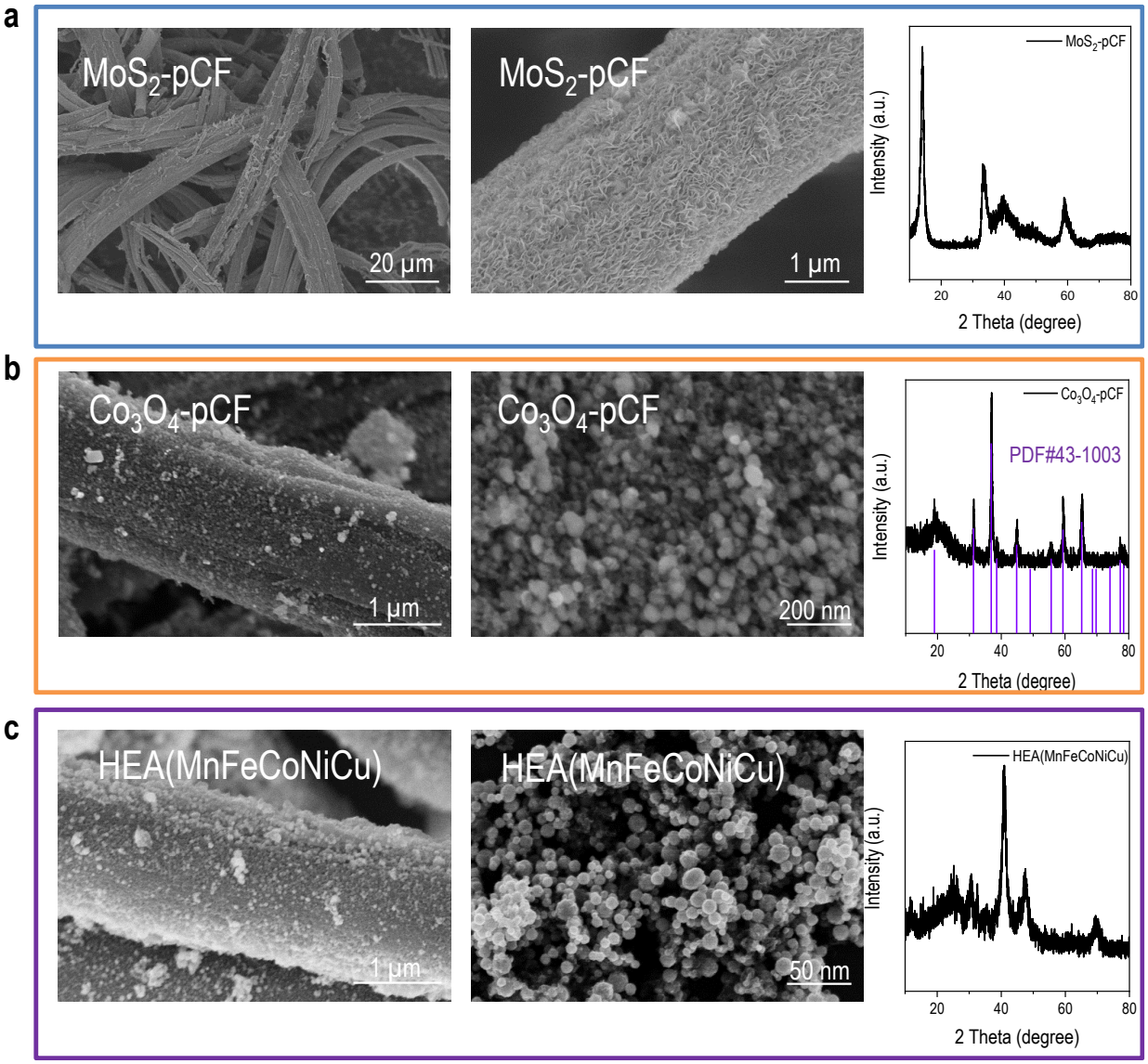

Fig. S1 (a) Loading of MoS_2 onto CFs. Metal sulfides (e.g., MoS_2) can be uniformly and stably anchored onto the surface of CFs owing to the abundant anchoring functional groups of CFs. (b) Loading of metal oxides onto CFs (e.g., Co_3O_4). Co_3O_4 can be uniformly and stably anchored onto the surface of CFs owing to the abundant anchoring functional groups of CFs. (c) High-entropy alloy NPs loaded on a single CF. Metal precursors (Mn, Fe, Co, Ni, and Cu) can coordinate with the abundant oxygen-containing functional groups on CFs to form polymetallic coordination precursors. After pyrolysis, metal precursors transform into uniformly distributed high entropy alloy NPs.

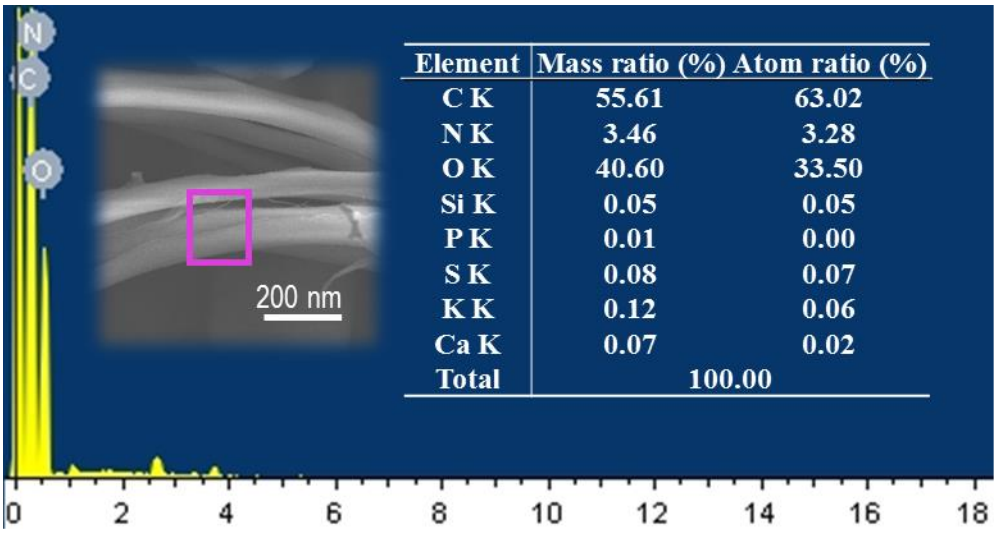

Element	Mass ratio (%)	Atom ratio (%)
C K	55.61	63.02
N K	3.46	3.28
O K	40.60	33.50
Si K	0.05	0.05
P K	0.01	0.00
S K	0.08	0.07
K K	0.12	0.06
Ca K	0.07	0.02
Total	100.00	

Fig. S2 Elemental composition characterization of CFs. CFs mainly consist of three elements: C, N, and O. Other elements (Si, P, S, K, and Ca) are present at a total low concentration of <0.4 at%, and most of them are inactive for catalytic reactions (e.g., Si, K, and Ca). These findings confirm the high purity of CFs as a biomass material.

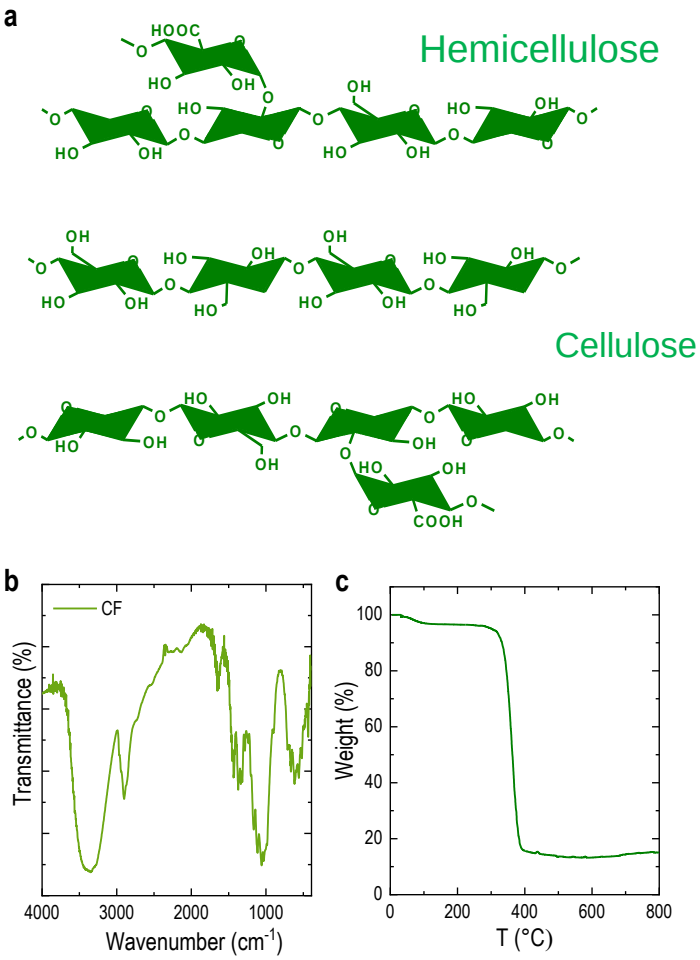

Fig. S3 Cotton fibers (a) Hierarchical structure of CFs. (b,c) FTIR spectrum (b) and TG curve (c) of CFs. CFs generally consist of cellulose and hemicellulose. CFs are primarily composed of varying types of carbohydrates in the forms of cellulose, hemicellulose, pectin, lignin, and sugar, and also of small amounts of proteins, waxes, and other inorganics. Fig. S2 shows the representative FT-IR spectra in the 3 800–400 cm^{-1}[4]. The first mass loss observed in the TG curve from room temperature to about 280 °C is attributed to the dehydration of the biomass. The second mass loss occurring between 250 and 400 °C, wherein the biomass undergoes rapid thermal degradation, corresponds to the decomposition of organic components such as cellulose, hemicellulose, and lignin. The pyrolysis produces a large amount of volatiles, which is conducive to generating pore structures.

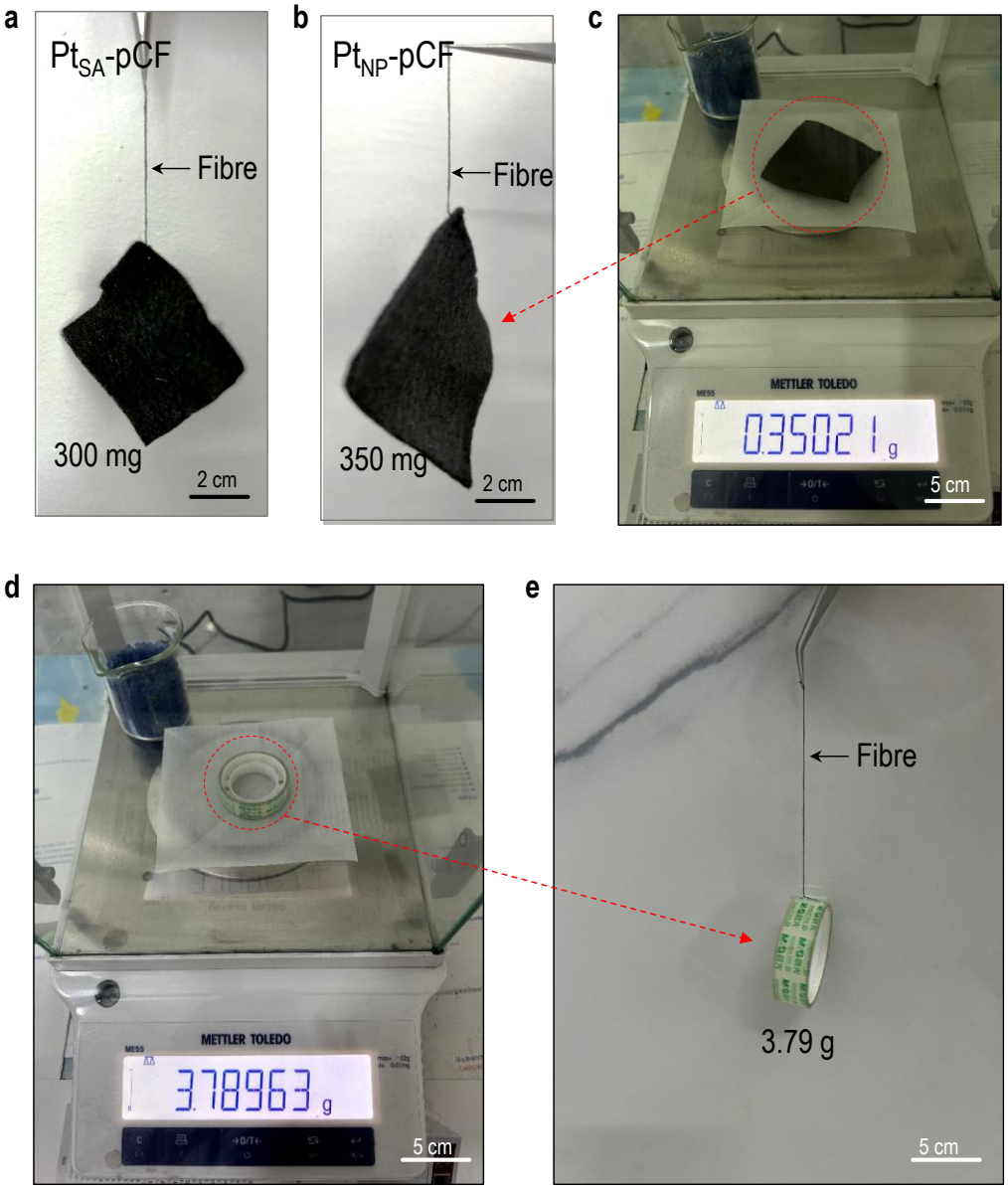

Fig. S4 (a,b) Pyrolyzed cotton fabric mat held by a single fiber. (c) The mass of a piece of Pt_{SA}-pCF. (d,e) The weight that a single cotton fiber can withstand.

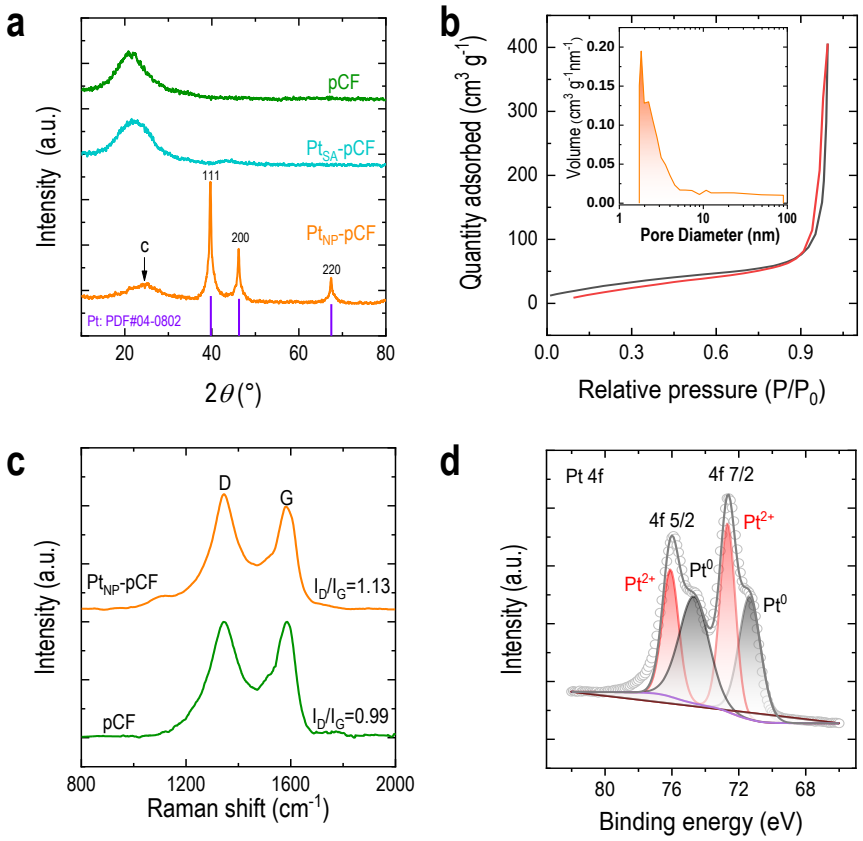

Fig. S5 Structural and atomic-level characterization of the Pt$_{NP}$–pCF catalysts. (a) X-ray diffraction (XRD) patterns of pCF, Pt$_{SA}$–pCF and the Pt$_{NP}$–pCF composites. (b) Nitrogen adsorption–desorption isotherms of Pt$_{NP}$–pCF (Illustrated as pore size distributions of Pt$_{NP}$–pCF). (c) Raman spectra of Pt$_{NP}$–pCF, and pCF. (d) High-resolution X-ray photon spectroscopy (XPS) spectra of Pt 4f of Pt$_{NP}$–pCF.

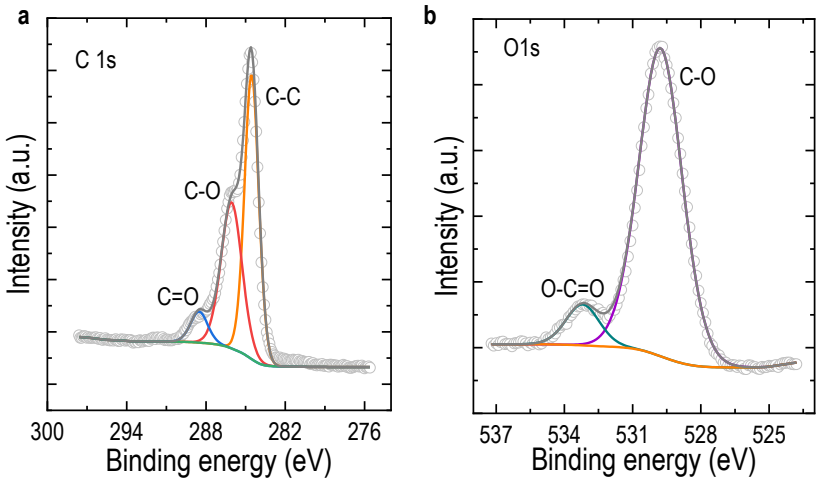

Fig. S6 Chemical characterization of Pt_{NP}-pCF. (a) HR-XPS spectra of C 1s in Pt_{NP}-pCF (b) and O 1s in Pt_{NP}-pCF.

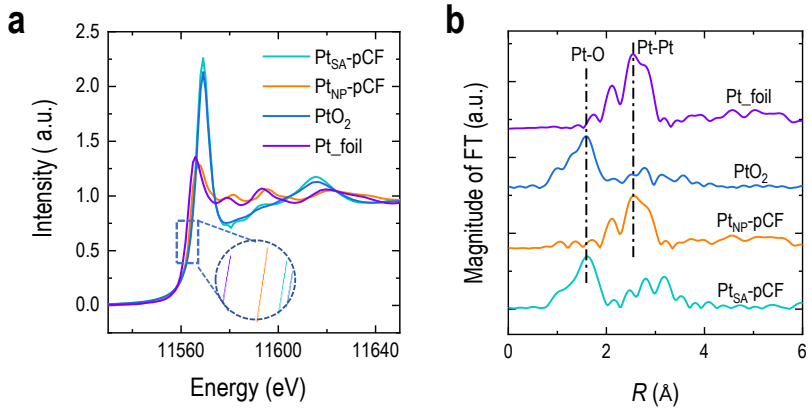

Fig. S7 (a) and (b) L-edge X-ray absorption near edge structure (XANES) spectra (a) and Fourier-transformed L-edge extended X-ray absorption fine structure (EXAFS) spectra (b) of the platinum in PtSA–pCF, PtNP–pCF, PtO_2, and Pt_foil.

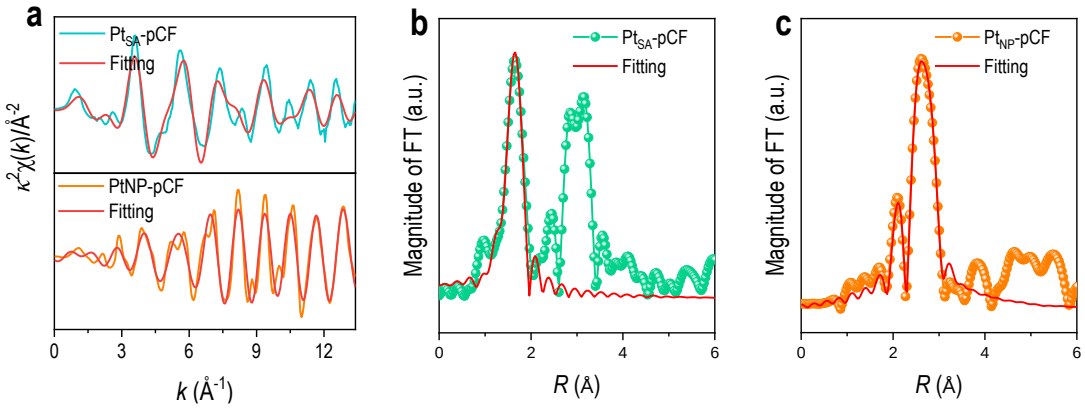

Fig. S8 (a) Fourier-transformed magnitudes of Pt L-edge EXAFS spectra in k space for Pt_{SA}-pCF and Pt_{NP}-pCF. Fourier-transformed magnitudes of Pt L-edge EXAFS spectra in R space for Pt_{SA}-pCF (b) and Pt_{NP}-pCF (c).

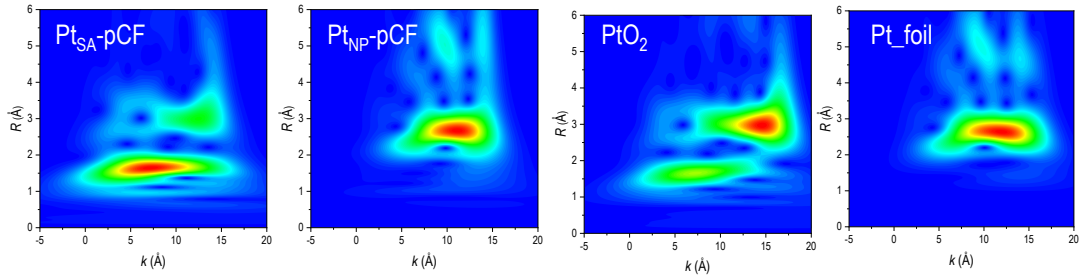

Fig. S9 Wavelet transform (WT) analysis of Pt_{SA}-pCF, Pt_{NP}-pCF, PtO_2, and Pt_foil.

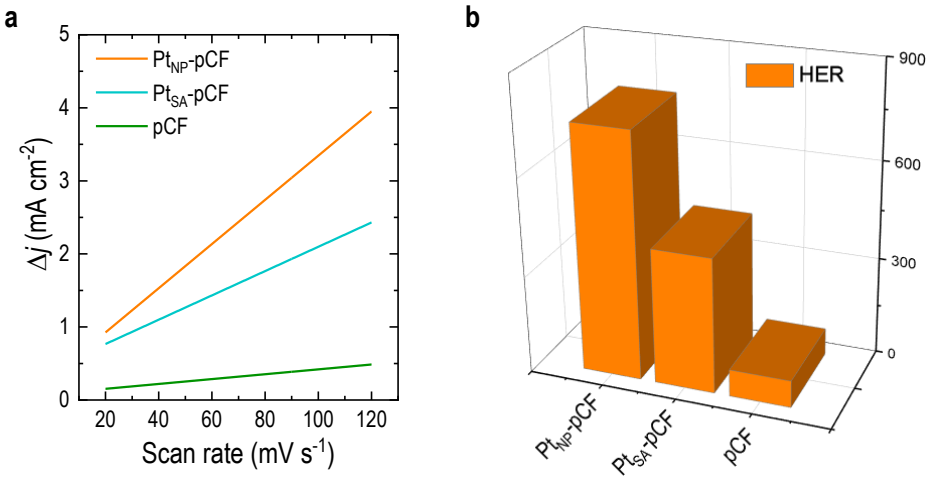

Fig. S10 Electrocatalytic HER activity of different catalysts. (a, b) C_{dl} (a) and calculated ECSA values (cm^{-2}) of HER (b) of Pt_{NP}-pCF, Pt_{NP}-pCF, and pCF catalysts in 1 M KOH.

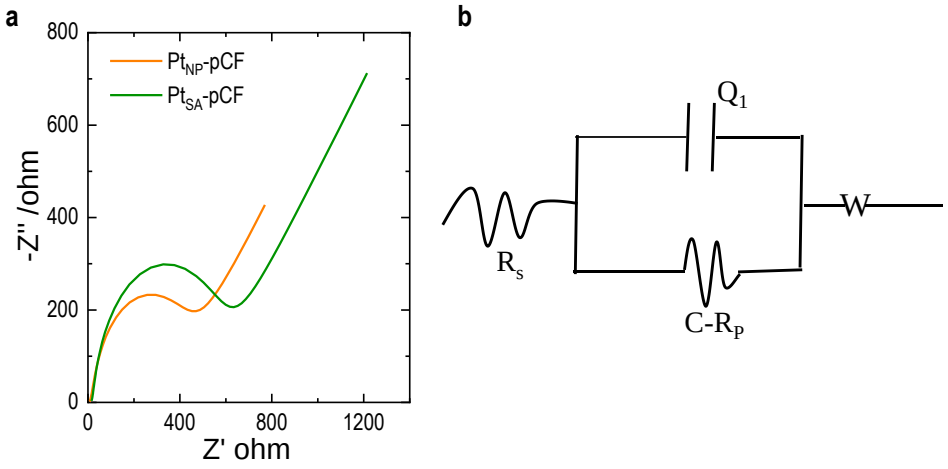

Fig. S11 Electrocatalytic HER activity of different catalysts. (a) Nyquist plots of HER. (b) Equivalent electrical circuit of the studied catalysts in 1 M KOH.

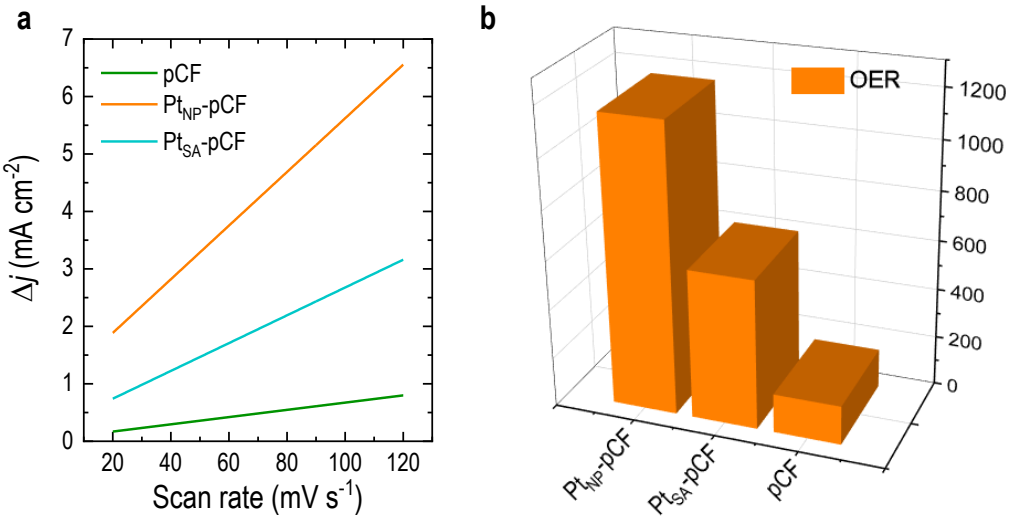

Fig. S12 Electrocatalytic OER activity of different catalysts. (a, b) C_{dl} (a) and calculated ECSA values (cm^{-2}) of OER (b) of Pt_{NP}-pCF, Pt_{NP}-pCF, and pCF catalysts in 1 M KOH.

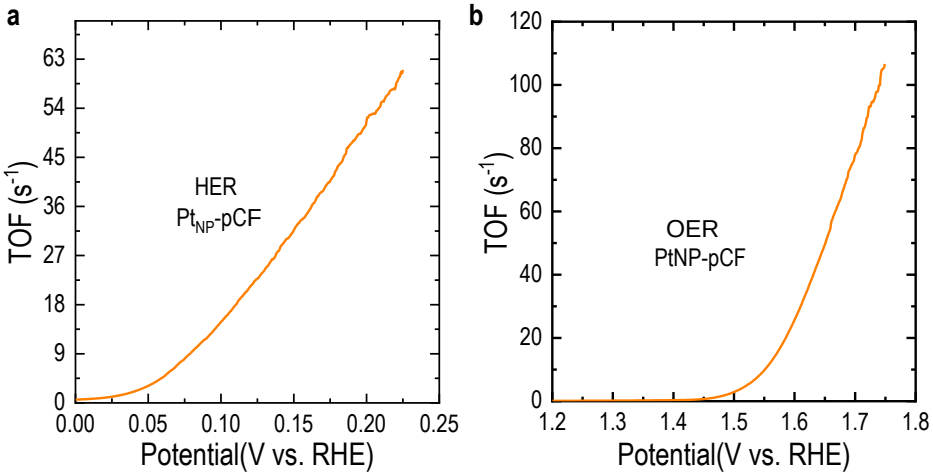

Fig. S13 TOF of HER and OER processes catalyzed by Pt_{NP}-pCF. (a,b) TOF of Pt sites in Pt_{NP}-pCF for HER (a) and OER (b) in 1 M KOH.

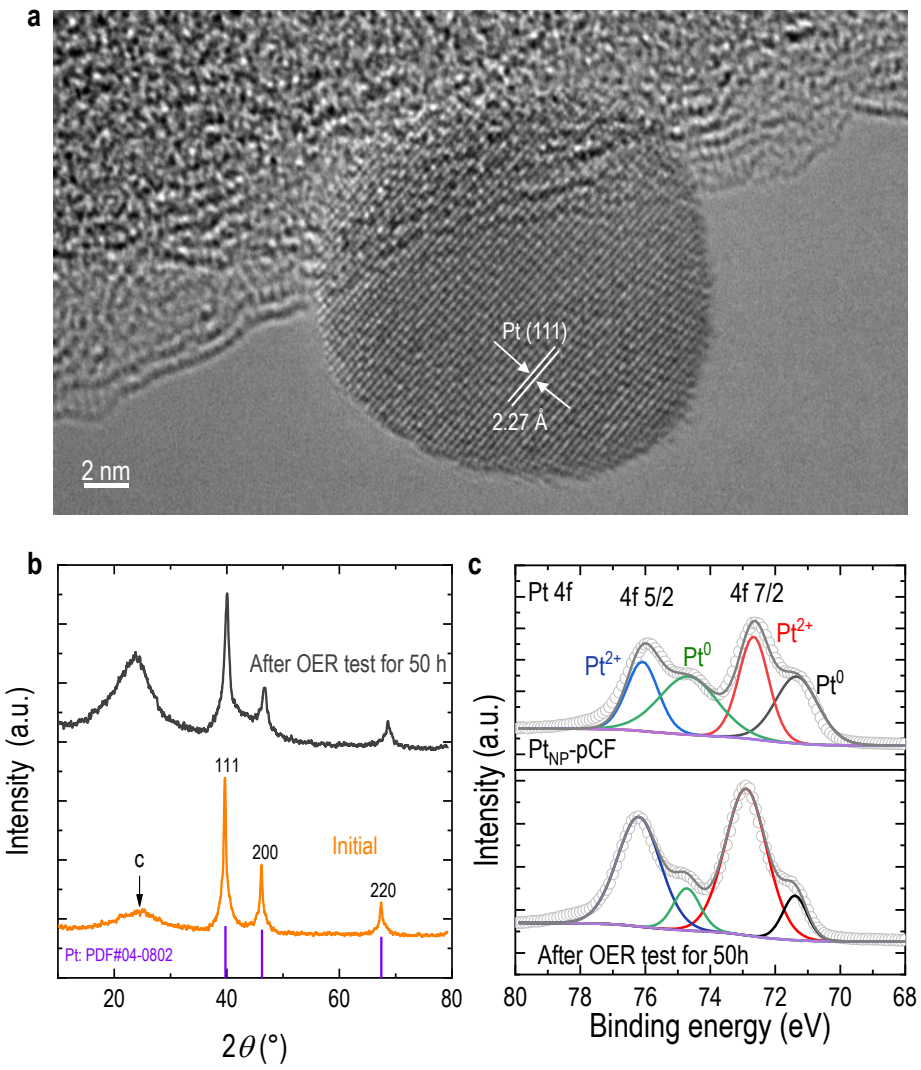

Fig. S14. (a) TEM images of the Pt_{NP}-pCF catalyst after the OER stability test (340 mV for 50 h). (b) XRD spectra of Pt_{NP}-pCF catalyst before and after the OER test (320 mV for 50 h). (c) HR-XPS spectra of Pt_{NP}-pCF after OER test at 320 mV for 50 h for Pt 4f.

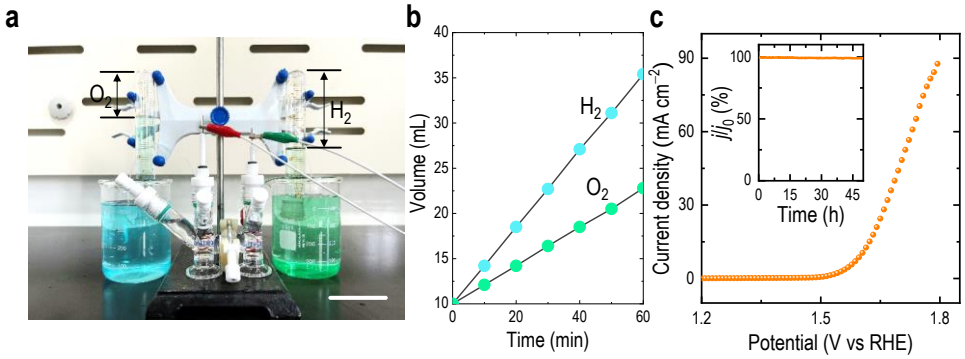

Fig. S15 (a) Photograph of a water splitting system. Scale bar is 5 cm. (b) Volumes of generated O_2 and H_2 during the water splitting process. (c) Polarization curve and stability test (inset) of the water splitting system based on Pt_{NP}-pCF.

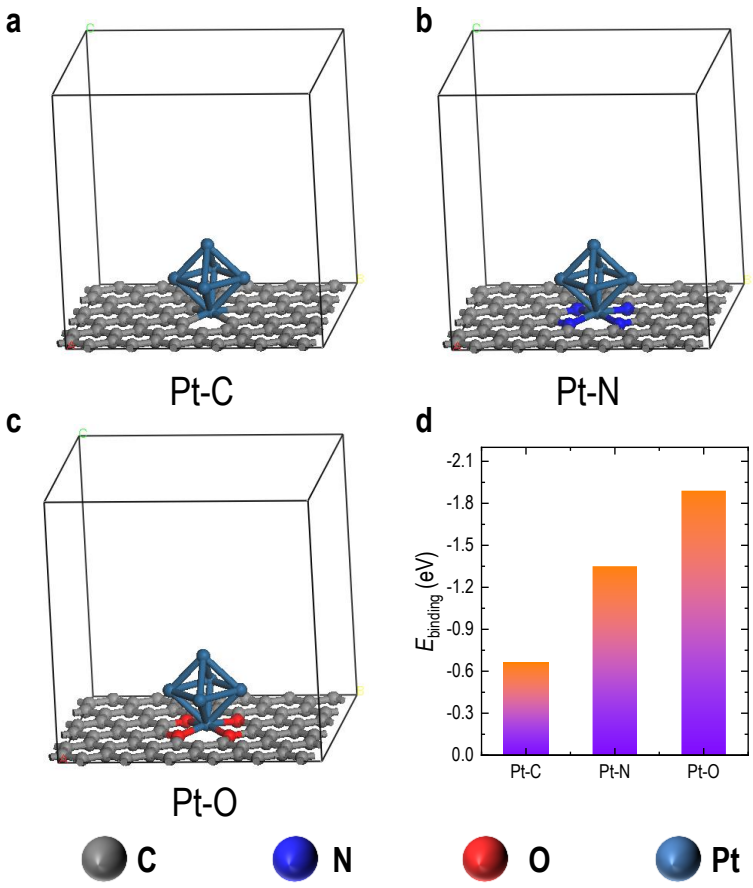

Fig. S16 DFT models of Pt NP on the doped graphene matrix with different anchors (C, N, O). (a) Carbon anchor. (b) Nitrogen anchor. (c) Oxygen anchor (i.e., the proposed anchoring mechanism in this work). (d) Calculated binding energies between the cobalt atom and the anchors (C, N, O), which suggests that oxygen has a higher binding interaction than the control samples.

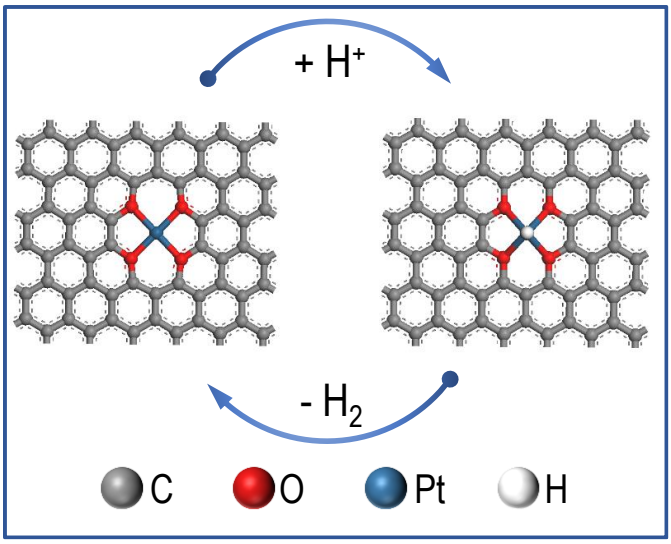

Fig. S17 Theoretical analysis. HER mechanisms (top view).

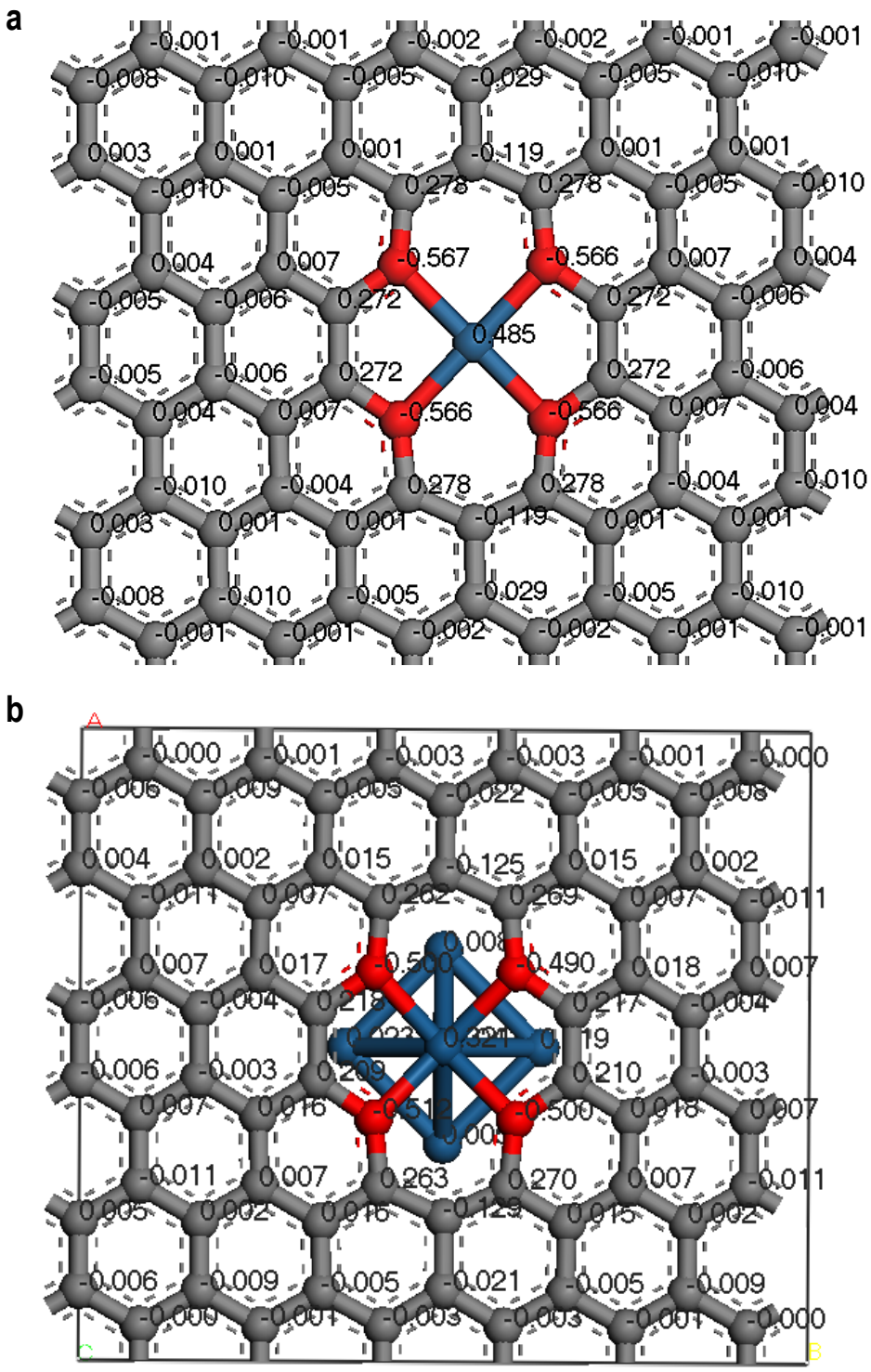

Fig. S18 Mulliken charge distributions of (a) Pt_{SA}-pCF and (b) Pt_{NP}-pCF.

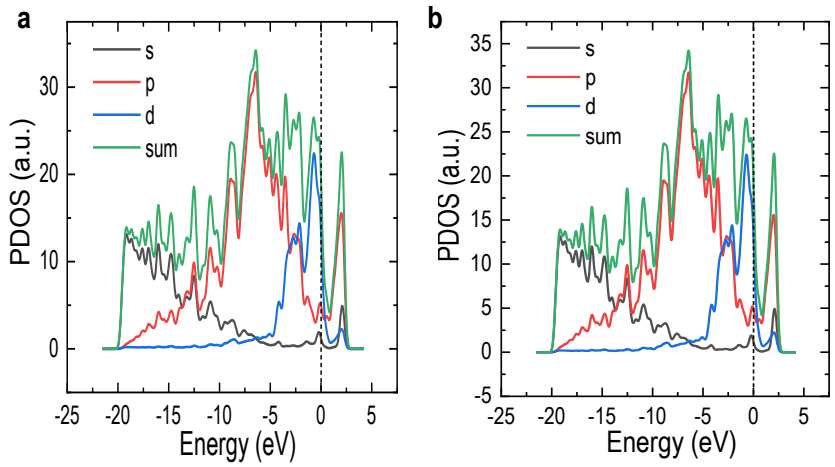

Fig. S19 Theoretical analysis. Calculated total and partial density of states of (a) Pt_{NPSA}-pCF, and (b) Pt_{SA}-pCF. Dash lines represent the Fermi level.

6 Supplemental tables

Table S1. The atomic ratio of elements in Pt_{SA}-pCF and Pt_{NP}-pCF.

Sample	Pt_{SA}-pCF	Pt_{NP}-pCF
Amount of Pt	0.76%	8.65%

Table S2. Fitted results of Pt L-edge EXAFS curves.

Sample	Shell	N[a]	R[b]	σ^2(Å^2)[c]	R factor (%)[d]
Pt_Foil[e]	Pt-Pt	1.14	2.770±0.007	0.0045±0.0007	0.0008
PtO_2[f]	Pt-O	2.40	2.002±0.0087	0.0036±0.0043	0.0074
Pt_{SA}-pCF[g]	Pt-O	3.56	2.014±0.0978	0.0032±0.0011	0.0127
Pt_{NP}-pCF-C[h]	Pt-Pt	1.25	2.761±0.0035	0.0044±0.0007	0.0181

[a]N, coordination number; [b]R, the distance between absorber and backscatter atoms; [c]σ^2, Debye-Waller factor to account for both thermal and structural disorders; [d]R factor indicates the goodness of the fit; [e]Fitting range: $1.00 \le k(Å) \le 13.00$ and $2.00 \le R(Å) \le 3.00$; [f]Fitting range: $3.00 \le k(Å) \le 10.00$ and $1.00 \le R(Å) \le 2.00$; [g]Fitting range: $3.00 \le k(/Å) \le 14.00$ and $1.00 \le R(Å) \le 2.00$; [h]Fitting range: $1.70 \le k(/Å) \le 8.00$ and $1.00 \le R(Å) \le 2.00$; [i]Fitting range: $1.70 \le k(/Å) \le 8.10$ and $1.00 \le R(Å) \le 2.00$; [j]Fitting range: $2.00 \le k(/Å) \le 12.000$ and $1.00 \le R(Å) \le 2.00$. [k]Fitting range: $2.00 \le k(/Å) \le 12.13$ and $1.00 \le R(Å) \le 2.00$.

Table S3. Binding energies of cobalt with the heteroatoms (C, N, O) doped in the graphene matrix.

Anchor	C	N	O
E (eV)	−0.66	−1.35	−1.89

Note: We use the equation $E = E_{total} - E_G - E_{PtNP} + E_{anchor}$ to calculate the binding energies of Pt NPs at the three anchor sites. E_{total} denotes the energy of the simulation cell; E_G denotes the energy of the doped graphene matrix; E_{PtNPs} denotes the energy of the Pt NPs component; E_{anchor} denotes the energy of a single anchor atom (i.e., C, N, and O). A more negative value of E indicates a stronger and thus more stable binding.

7 Supplemental References

1 N. Logeshwaran, S. Ramakrishnan, S. S. Chandrasekaran, M. Vinothkannan, A. R. Kim, S. Sengodan, D. B. Velusamy, P. Varadhan, J. H. He and D. J. Yoo, *Appl. Catal. B*, 2021, **297**, 120405.

2 M. D. Segall, P. J. D. Lindan, M. J. Probert, C. J. Pickard, P. J. Hasnip, S. J. Clark and M. C. Payne, *J. Phys. Condens. Matter*, 2002, **14**, 2717–2744.

3 S. Grimme, *J. Comput. Chem.*, 2006, **27**, 1787.

4 Z. Q. He, Y. L. Liu, H. J. Kim, H. Tewolde, H. L. Zhang, *J. Cotton Res.*, 2022, **5**, 11.